A Component of Excitation-Contraction Coupling Triggered in the Absence of the T671-L690 and L720-Q765 Regions of the II-III Loop of the Dihydropyridine Receptor α_{1S} Pore Subunit

Chris A. Ahern, Dipankar Bhattacharya, Lindsay Mortenson, and Roberto Coronado
Department of Physiology, University of Wisconsin School of Medicine, Madison, Wisconsin 53706 USA

ABSTRACT We conducted a deletion analysis of two regions identified in the II-III loop of α_{1S}, residues 671–690, which were shown to bind to ryanodine receptor type 1 (RyR1) and stimulate RyR1 channels in vitro, and residues 720–765 or the narrower 724–743 region, which confer excitation-contraction (EC) coupling function to chimeric dihydropyridine receptors (DHPRs). Deletion mutants were expressed in dysgenic α_{1S}-null myotubes and analyzed by voltage-clamp and confocal fluo-4 fluorescence. Immunostaining of the mutant subunits using an N-terminus tag revealed abundant protein expression in all cases. Furthermore, the maximum recovered charge movement density was >80% of that recovered by full-length α_{1S} in all cases. Δ671–690 had no effect on the magnitude of voltage-evoked Ca^{2+} transients or the L-type Ca^{2+} current density. In contrast, Δ720–765 or Δ724–743 abolished Ca^{2+} transients entirely, and L-type Ca^{2+} current was reduced or absent. Surprisingly, Ca^{2+} transients and Ca^{2+} currents of a moderate magnitude were recovered by the double deletion mutant Δ671–690/Δ720–765. A simple explanation for this result is that Δ720–765 induces a conformation change that disrupts EC coupling, and this conformational change is partially reverted by Δ671–690. To test for Ca^{2+}-entry independent EC coupling, a pore mutation (E1014K) known to entirely abolish the inward Ca^{2+} current was introduced. α_{1S} Δ671–690/Δ720–765/E1014K expressed Ca^{2+} transients with Boltzmann parameters identical to those of the Ca^{2+}-conducting double deletion construct. The data strongly suggest that skeletal-type EC coupling is not uniquely controlled by α_{1S} 720–765. Other regions of α_{1S} or other DHPR subunits must therefore directly contribute to the activation of RyR1 during EC coupling.

INTRODUCTION

Skeletal muscle cells respond to membrane depolarization with an elevation in cytosolic Ca^{2+} that develops almost instantaneously and is proportional to the duration of the stimulus (Kim and Vergara, 1998). Two molecular complexes responsible for coupling membrane excitation to Ca^{2+} elevation are the dihydropyridine receptor (DHPR) in the transverse tubular membrane and the ryanodine receptor type 1 (RyR1) in the sarcoplasmic reticulum (SR) membrane (Block et al., 1988). Membrane depolarization is thought to increase the SR Ca^{2+} permeability by a conformational change transmitted from the DHPR to the RyR1 via protein-protein interactions. The processes that couple the movement of electrical charges in the DHPR to the opening of the RyR1 channel have been under close scrutiny for many years (Rios and Pizarro, 1991; McPherson and Campbell, 1993; Coronado et al., 1994; Meissner, 1994; Sutko and Airey, 1996; Franzini-Armstrong and Protasi, 1997).

A critical structural determinant of excitation-contraction (EC) coupling in skeletal muscle is the cytosolic loop between repeats II and III of the DHPR pore subunit α_{1S} (Fig. 1 *A*). The II-III loop, under the influence of membrane depolarization, has been suggested to trigger the release of Ca^{2+} from the SR (Tanabe et al., 1990; Garcia et al., 1994). The II-III loop would thus function as a surrogate "gating particle" which, after acquiring the correct conformation, becomes a catalyst for the energetically unfavorable opening of the RyR1 channel. Such a view represents a molecular version of the mechanical plunger model suggested earlier by Chandler et al., (1976). A prediction of this model is that the II-III loop must contain molecular motifs essential for activation of the RyR1 channel. A search for different regions of the II-III loop that affect RyR1 channel activity was conducted using recombinant and synthetic peptides (Lu et al., 1994; El Hayek et al., 1995; O'Reilly and Ronjat, 1999; Dulhunty et al., 1999; Gurrola et al., 1999; Casarotto et al., 2000). The strongest stimulation of RyR1 channels in vitro was produced by a synthetic peptide corresponding to α_{1S} residues 671–690. A second peptide, α_{1S} 724–760, had low stimulatory activity, but inhibited the stimulatory activity of the α_{1S} 671–690 peptide when both synthetic peptides were presented to RyR1-containing skeletal SR vesicles (El Hayek et al., 1995). These biochemical studies suggest that the region of the II-III loop encompassed by α_{1S} 671–690 could be the structural element of the II-III loop that triggers EC coupling in the muscle cell (El Hayek et al., 1998).

A second region of the II-III loop critical for EC coupling was identified in dysgenic myotubes by functional expression of chimeric cDNAs for DHPR pore subunits (Nakai et al., 1998). This study showed that a chimera consisting of a cardiac α_{1C} subunit with α_{1S} 720–765 replacing the homologous cardiac region expressed voltage-evoked Ca^{2+} transients of near-normal amplitude. The narrower α_{1S} 725–742

Received for publication 13 June 2001 and in final form 5 September 2001.
Address reprint requests to Dr. Roberto Coronado, Department of Physiology, University of Wisconsin, 1300 University Ave., Madison, WI 53706. Tel.: 608-263-7487; Fax: 608-265-5512; E-mail: coronado@physiology.wisc.edu.

0006-3495/01/12/3294/14 $2.00

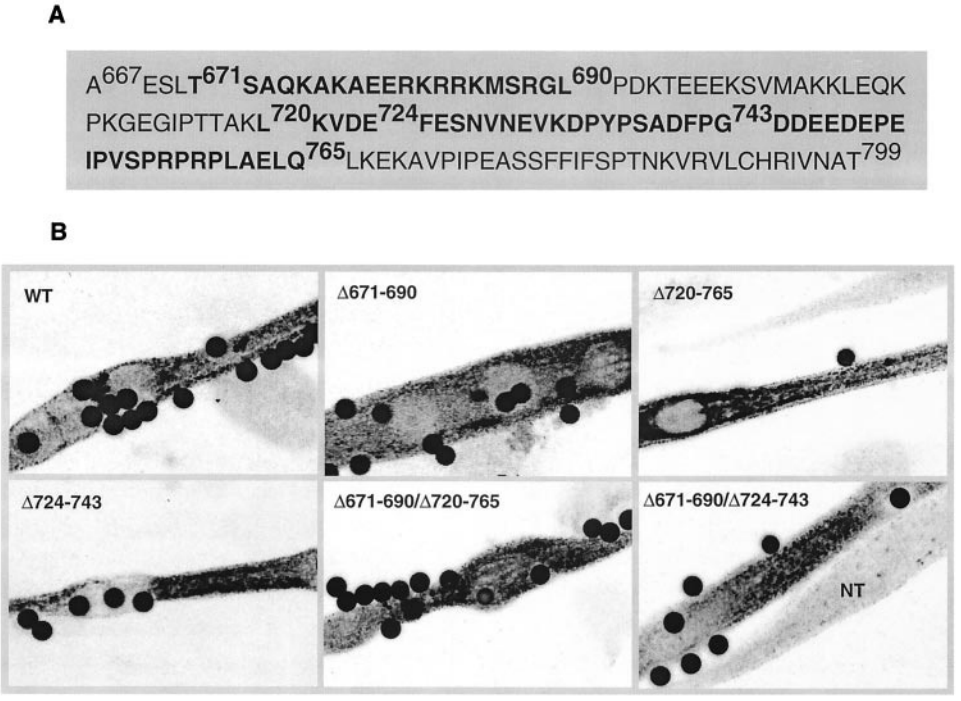

FIGURE 1 (*A*) Putative α_{1S} II-III loop according to a sequence lineup of Perez-Reyes and Schneider (1994). Residues in bold indicate deleted regions. (*B*) Confocal immunofluorescence of dysgenic myotubes expressing II-III loop deletions. Cells were transfected with CD8 cDNA plus the indicated construct; 3 to 5 days after transfection, cells were incubated with CD8 antibody beads, fixed, and stained with anti-T7 primary/fluorescein-conjugated secondary antibodies. Pixel intensity was converted to a 16-level inverted gray scale with high-intensity pixels in black. WT indicates full-length α_{1S} used as control. NF indicates a nontransfected myotube in the same focal plane of the transfected cell. Images are 50 × 80 μm and on-focus beads are 4.5 μm in diameter.

region recovered a slightly lower than normal Ca^{2+} transient. Furthermore, the Ca^{2+} transients in each case persisted in the presence of Ca^{2+} channel blockers, indicating recovery of skeletal-type EC coupling by the chimeras. Thus the two screening strategies, namely peptide analysis in vitro (El Hayek et al., 1995) and chimera analysis in situ (Nakai et al., 1998), arrived at different conclusions regarding the regions of the II-III loop essential for EC coupling function. To gain more decisive information on the EC coupling domains encoded by the II-III loop, we used a deletion strategy. The data clearly show that α_{1S} 720–765 is essential, but α_{1S} 671–690 can be deleted without a critical loss of function. However, deletion of both regions, which amounts to a loss of ~50% of the II-III loop sequence, does not entirely eliminate skeletal-type EC coupling. This result suggests that regions outside the II-III loop could contribute directly to the mechanism that activates RyR1 during EC coupling. Part of these results were published in abstract form (Ahern et al., 2001a).

MATERIALS AND METHODS

Primary cultures and cDNA transfection

Outbred Black Swiss mice (Charles River, MA) were used to generate colonies of heterozygous dysgenic ($\alpha_{1S}^{+/mdg}$) and dyspedic ($RyR1^{\pm}$) mice that were genotyped by PCR. $RyR1^{\pm}$ mice were a gift of Dr. H. Takeshima; α_{1S} null ($\alpha_{1S}^{mdg/mdg}$) or RyR1 null ($RyR1^{-/-}$) mice were generated by interbreeding of heterozygous parents. Primary cultures were prepared from enzyme-digested hindlimbs of late-gestation (E18) $\alpha_{1S}^{mdg/mdg}$ or $RyR1^{-/-}$ fetuses as described (Beurg et al., 1997). cDNAs of interest and a separate plasmid encoding the T-cell membrane antigen CD8 were mixed at a 1:1 weight ratio and cotransfected with the polyamine LT-1 (Panvera, WI). CD8-transfected cells were recognized by incubation with anti-CD8 antibody beads (Dynal, Norway). Determined by immunostaining, ~80% of the CD8-transfected dysgenic α_{1S} null myotubes coexpressed the α_{1S} cDNA of interest.

α_{1S} II-III loop deletions

All cDNA constructs were sequenced at least twice using BigDye technology (Perkin-Elmer, CA) at a campus facility. For epitope tagging and expression in mammalian cells, the unmodified full-length rabbit α_{1S} cDNA encoding residues 1–1873 (Genebank M23919 nucleotide coordinates nt 226 to nt 5847) was fused in frame to the first 11 amino acids of the phage T7 gene 10 protein in the mammalian expression vector pSG5 (Stratagene, CA) using *Age*I and *Not*I cloning sites. All constructs were made using the T7-tagged α_{1S} as template in PCR-based strategies. Genebank M23919 nucleotide coordinates are used below to describe primers. A silent *Hind*III site was introduced by PCR at nt 2228 in the full-length α_{1S} template and cloned into the T7-α_{1S} pSG5 vector using *Age*I and *Xho*I sites. The *Hind*III-*Xho*I fragment (nt 2228 to nt 2878) encompassing the II-III loop was subcloned into pCR 2.1 TOPO TA (Invitrogen, CA) and this plasmid was further used for PCR reactions. PCR reactions consisted of 10 ng pCR 2.1 TOPO/*Hind*III-*Xho*I insert, 15 pmol of each primer, 0.5 mM

TABLE 1 Ca^{2+} conductance, charge movement, and Ca^{2+} transients of α_{1S} deletion mutants

	Q-V			$\Delta F/F$-V			G-V		
	Q_{max} (fC/pF)	$V_{1/2}$ (mV)	k (mV)	$\Delta F/F_{max}$	$V_{1/2}$ (mV)	k (mV)	G_{max} (pS/pF)	$V_{1/2}$ (mV)	k (mV)
α_{1S} null	0.8 ± 0.2* (12)	−1.7 ± 3.7*	11.9 ± 2.2*	— (24)	—	—	— (45)	—	—
RyR1 null	3.9 ± 0.5* (9)	17.4 ± 4.5	15.9 ± 1.0*	—	—	—	31.3 ± 6.1* (9)	11.6 ± 3.0	6.3 ± 0.5
Δ671–690	5.4 ± 0.5 (6)	15.5 ± 1.9	20.3 ± 2.2	3.1 ± 0.4 (8)	10.9 ± 1.6	11.2 ± 1.0	105 ± 9.2 (6)	30.5 ± 3.5	4.3 ± 1.1
Δ720–765	5.5 ± 0.8 (6)	21.0 ± 5.6	24.7 ± 1.7	— (7)	—	—	— (13)	—	—
Δ724–743	5.5 ± 0.5 (4)	14.0 ± 2.3	17.9 ± 0.9	— (8)	—	—	— (8)	—	—
Δ671–690/ Δ720–765	5.3 ± 0.8 (5)	21.5 ± 5.5	21.3 ± 2.0	0.5 ± 0.1* (13)	9.5 ± 4.5	9.5 ± 0.6	63.8 ± 7.1* (5)	31.5 ± 1.6	6.5 ± 0.5
Δ671–690/ Δ724–743	6.2 ± 1.3 (4)	15.3 ± 5.4	18.1 ± 2.6	— (9)	—	—	79.2 ± 6.3* (6)	28.8 ± 2.7	5.8 ± 0.6
WT	6.3 ± 0.2 (6)	16.7 ± 3.5	19.6 ± 1.4	2.9 ± 0.4 (11)	11.0 ± 1.9	8.4 ± 1.0	109.5 ± 8.3 (7)	25.5 ± 2.1	4.9 ± 0.7

Entries correspond to mean ± SEM of Boltzmann parameters fitted to each cell. The number of cells is in parentheses. Conflocal fluo-4 fluorescence change ($\Delta F/F < 0.2$) or L-type Ca^{2+} current (<20 pA/cell) were not detectable in the indicated number of cells.

*Data compared to control (WT) with t-test significance $p < 0.05$. One-way ANOVA of Q_{max}, $Q_{1/2}$, Q_k, $\Delta F/F_{1/2}$, $\Delta F/F_k$, $G_{1/2}$, and G_k of II–III loop deletion constructs and WT had significance $p > 0.18$. Excluded from the conductance averages are two cells expressing Δ671–690/Δ720–765 that had undetectable L-type Ca^{2+} current, but large charge movements (Q_{max} = 4.9 and 4.6 fC/pF).

dNTPs, 1X cloned Pfu buffer (Stratagene) and 2.5U cloned Pfu DNA polymerase (Stratagene). Amplification was carried out for 30 cycles at 95°C for 45 s, 60°C for 2 min, and 72°C for 2 min/kb of plasmid. The PCR reaction was treated with 10U of *Dpn*I (Stratagene) and recircularized with T4 DNA ligase (Stratagene). Once amplified by PCR, the *Hind*III-*Xho*I digest was ligated into the T7-α_{1S} pSG5 vector using the same restriction sites. HPLC-purified primers (Operon, CA) were used in all PCR reactions and were as follows: for Δ671–690 the antisense primer was complementary to nt 2202 to nt 2235 and the sense primer was nt 2296 to nt 2326; for Δ720–765 the antisense primer was complementary to nt 2340 to nt 2382 and the sense primer was nt 2521 to nt 2545; for Δ724–743 the antisense primer was complementary to nt 2351 to nt 2394 and the sense primer was nt 2455 to nt 2482. A phosphate was tagged to the 5′-end of the sense primer to recircularize the amplified TOPO vector. Double deletions Δ671–690/Δ720–765 and Δ671–690/Δ724–743 were produced sequentially such that a pCR 2.1 TOPO vector with a *Hind*III-*Xho*I insert carrying a deletion of nt 2236 to nt 2295 (α_{1S} residues 671–690) was used as template for the second deletion using the same primers above.

Δ671–690/Δ720–765/E1014K

The *Xho*I-*Bgl*II fragment of the unmodified α_{1S} template encompassing residue E1014 (nt 2878 to nt 4712) was subcloned into a pCR 2.1 TOPO TA vector. For the pore mutation, mismatches were introduced at nt 3265 (g3265a) for the E1014K substitution, and at nt 3297 (a3297c) and nt 3300 (c3300t) for the introduction of a unique *Cla*I site for identification of E1014K clones. With these modifications, the sequence of the antisense primer was 5′CCTCCTCGTTGGA*A*TC*G*ATGGCCCTGTACAGCA-GCTGGGGCCATCCCT*T*GAAGG 3′ (italics are mismatched bases). The sense primer was nt 3314 to nt 3349. The E1014K-substituted *Xho*I-*Bgl*II fragment was ligated using *Xho*I and *Bgl*II sites in the T7-pSG5 α_{1S} Δ671–690/Δ720–765 vector.

Whole-cell voltage-clamp

Cells were voltage-clamped 3 to 5 days after transfection. Transfected cells revealed by CD8 beads were voltage-clamped with an Axopatch 200B amplifier (Axon Instruments, CA) and a Digidata 1200 (Axon) pulse generator and digitizer. Linear capacitance, leak currents, and effective series resistance were compensated with the amplifier circuit. The charge movement protocol included a long prepulse to inactivate Na^+ channel ionic and gating currents (Strube et al., 1996). Voltage was stepped from a holding potential of −80 mV to −35 mV for 750 ms, then to −50 mV for 5 ms, then to the test potential for 50 ms, then to −50 mV for 30 ms and finally to the −80 mV holding potential. Test potentials were applied in decreasing order every 5 mV from +100 or +110 mV to −75 mV. The inter-test pulse period was 10 s. Nonlinear charge movement from a more negative holding potential, −120 mV, resulted in Q-V curves with the same maximum charge movement density. On-line subtraction of the linear charge was done by a P/4 procedure. The P/4 pulses were delivered immediately before the protocol from −80 mV in the negative direction. To verify that the P/4 pulses adequately subtracted the linear component of the charging current, we investigated the voltage-dependence of the cell membrane capacity in the range of −80 to −120 mV. In this range, the membrane capacity varied linearly with voltage, within a 0.5% error, in all cells investigated (>20 cells). Controls indicated that nontransfected dysgenic myotubes (see Table 1) had minimal charge movement and did not generate detectable Ca^{2+} transients. An overwhelming majority of these cells (45 of 47) did not express the low-density dysgenic Ca^{2+} current described elsewhere in dysgenic mice of a different genetic background (Strube et al., 1998). The voltage dependence of charge movements (Q), peak intracellular Ca^{2+} ($\Delta F/F$), and Ca^{2+} conductance (G), was fitted according to a Boltzmann distribution (Eq. 1) $A = A_{max}/(1 + \exp(-(V - V_{1/2})/k))$. A_{max} is Q_{max}, $\Delta F/F_{max}$, or G_{max}; $V_{1/2}$ is the potential at which $A = A_{max}/2$; and k is the slope factor.

Solutions

The external solution in all cases was (in mM): 130 TEA methanesulfonate, 10 $CaCl_2$, 1 $MgCl_2$, 10 HEPES titrated with TEA(OH) to pH 7.4. For Ca^{2+} transients and Ca^{2+} currents, the pipette solution was (in mM): 140 cesium aspartate, 5 $MgCl_2$, 0.1 EGTA (Ca^{2+} transients) or 5 mM EGTA (Ca^{2+} currents and specified Ca^{2+} transients), and 10 MOPS-CsOH pH 7.2. For

charge movements, the internal solution was (in mM): 120 NMG (*N*-methyl glucamine)-glutamate, 10 HEPES-NMG, 10 EGTA-NMG, pH 7.3 (Ahern et al., 2001b). For charge movements the external solution was supplemented with 0.5 mM $CdCl_2$ and 0.5 mM $LaCl_3$ to block the Ca^{2+} current and 0.05 mM TTX to block residual Na^+ current.

Confocal fluorescence microscopy

Confocal line-scan measurements were performed as described (Beurg et al., 1999a, b; Conklin et al., 2000). Cells were loaded with 4 mM fluo-4 AM (Molecular Probes, OR) for ~30 min at room temperature. When indicated, cells were dye-loaded through the patch pipette with internal solution supplemented with 1 mM fluo-4 (free acid). Dye fluorescence was imaged in an inverted Olympus microscope with a 20× objective (N.A. 0.4) and a Fluoview confocal attachment (Olympus, NY). Excitation light was provided by a 5 mW Argon laser attenuated to 6% with neutral density filters. In line-scan mode the line had a dimension of 512 pixels (0.3–0.4 μm/pixel) and the acquisition period of a single 512-pixel line was 2.05 ms.

Immunostaining

Transfected cells were kept in culture for 3 to 5 additional days and afterward fixed and processed for immunofluorescence (Beurg et al., 1999b; Ahern et al., 2001b). Controls shown elsewhere indicated that dysgenic myotubes do not express the *mdg* gene product, a truncated α_{1S}, at levels detectable by our immunostaining technique (Strube et al., 1998); α_{1S} was identified with a mouse monoclonal antibody against a T7 epitope fused to the N-terminus of the α_{1S} construct. The anti-T7 antibody (Novagen, Madison, WI) was used at a dilution of 1:1000. The secondary antibody was a fluorescein-conjugated goat anti-mouse IgG (Boehringer Mannheim, Indianapolis, IN) used at a dilution of 1:1000. Confocal images of immunofluorescence had a dimension of 1024 × 1024 pixels (0.35 μm/pixel) and were obtained with a 40× oil-immersion objective (N.A. 1.3). Images were Kalman-averaged three times and the pixel intensity displayed as 16 levels of gray in reverse. All images were acquired using minimal laser power and predetermined PMT settings to avoid pixel saturation and for accuracy in the comparison of images.

RESULTS

All constructs carried an 11-residue T7 tag at the N-terminus, which is useful for determining relative protein expression levels. Constructs were transiently expressed in dysgenic myotubes using the pSG5 mammalian expression vector and were identified by the deleted residues. A T7-tagged full-length α_{1S} expressed in dysgenic myotubes was used as control and was identified as WT. Fig. 1 *B* shows confocal images in reverse contrast of dysgenic myotubes fixed and immunostained with anti-T7 antibody and a fluorescein-conjugated secondary antibody. A CD8 cDNA was used as a transfection marker, and beads coated with an anti-CD8 antibody against an external epitope were used to identify transfected cells. In all the images, in-focus beads are 4.5 μm in diameter. For comparison, a nontransfected cell (NT) in the same confocal plane as the transfected cell is indicated next to the myotube expressing Δ671–690/Δ724–743. The overall T7 staining pattern varied between diffuse and punctate, with no correlation between the staining pattern and the expressed construct. We found abundant expression of each of the tested constructs in the periphery of the nuclei, which in the images appear as ellipsoids devoid of stain. Three nuclei in a row are evident in the myotube expressing Δ671–690. The perinuclear staining presumably corresponds to immature α_{1S} subunits trafficking through the endoreticular membrane network. We also found abundant staining in the periphery of the cell in areas clearly separated from the endoreticular network. This is most clear in the myotube expressing Δ720–765. The peripheral staining is entirely consistent with the known location of functional DHPRs in cultured myotubes. At these peripheral locations, couplings are established between the surface and SR membranes (Takekura et al., 1994).

To determine the density of voltage-sensors expressed by each construct we used a gating current protocol. The inset in each of the six panels of Fig. 2 shows intramembrane currents produced by the movement of charges in the expressed construct in response to a voltage step to +90 mV. The traces show transient outward current at the start of a 50-ms voltage step as the charges move in the outward direction (ON charge) followed by inward current at the end of the voltage step as charges return to the original position (OFF charge). We found a good correspondence between the magnitude of the ON and OFF components, as would be expected if charge movements were due to reversible displacements of intramembrane charges. The graphs in Fig. 2 show charge versus voltage relationships for six of the seven tested constructs obtained by integration of the OFF component, which usually was less contaminated by ionic current than the ON component. The voltage dependence of the mean charge was fit in each case to a Boltzmann equation (Eq. 1), which is indicated by the sigmoidal line. The background charge present in nontransfected cells is shown by the filled squares under the control curve of cells expressing full-length α_{1S} (WT, *top left panel*). In all cases, the near-maximum charge density measured at large positive potentials was 5 to 8-fold above the background density. At +100 mV, the experimental charge density was ~90% of the fitted Q_{max}, indicating that the chosen range of test pulses was adequate to detect the bulk of the nonlinear charge movements. This can be seen by comparing $Q_{exp}(+100)$ in Fig. 2 and Q_{max} in Table 1. A cell by cell analysis of the averages shown in Fig. 2 further confirmed that the fitted Boltzmann parameters (Q_{max}, $V_{1/2}$, k) were not significantly different from control (see Table 1). The similarity in Q_{max} indicated that the II-III loop deletions did not interfere with the voltage-sensing properties of the DHPR or the trafficking of the DHPR complex to the cell surface. Likewise, the similarity in midpoint potential ($V_{1/2}$) and steepness (k factor) suggested that the deletions were of minimal consequence for the electrical characteristics of the DHPR voltage sensor.

Depolarization-evoked Ca^{2+} transients are shown in Fig. 3. We measured the confocal fluorescence of fluo-4 in line-scan acquisition mode. A representative line-scan in

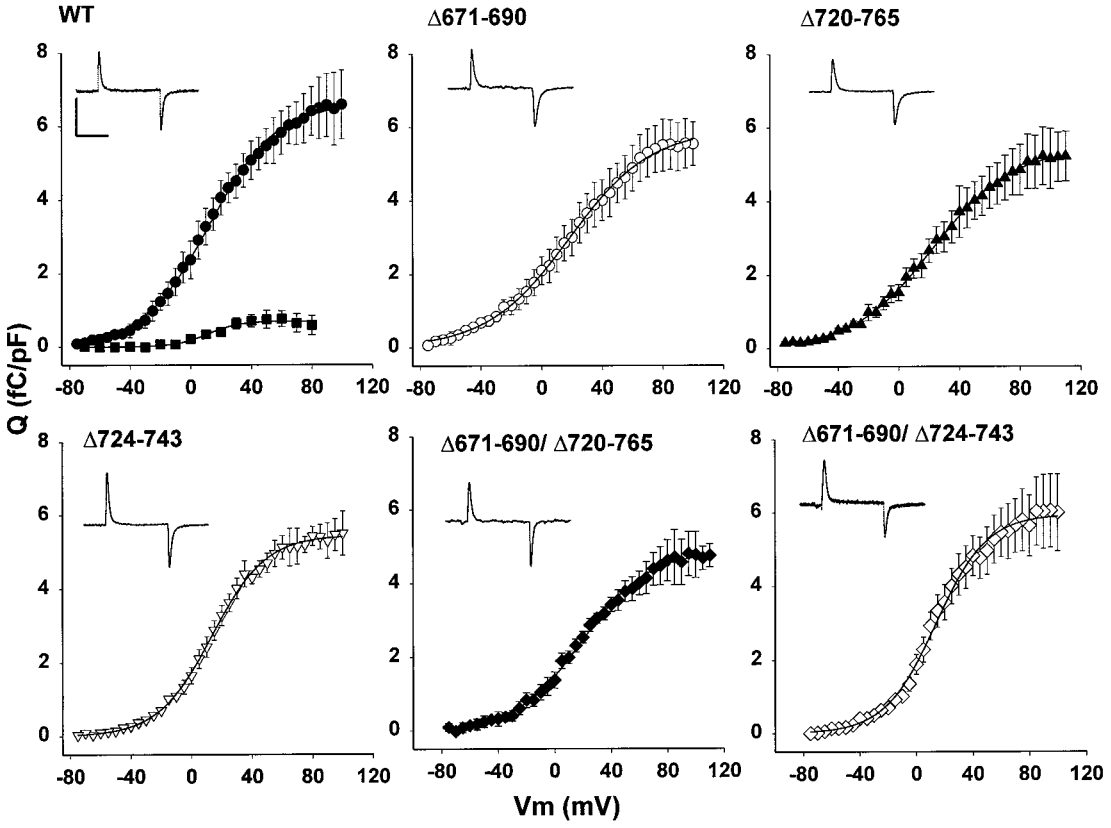

FIGURE 2 Intramembrane charge movements expressed by II-III loop deletions. The insets show nonlinear intramembrane current in dysgenic myotubes expressing the indicated construct. The test potential was to +90 mV with pre-test and post-test pulses indicated in Materials and Methods. The capacitance of each cell (in pF) is from left to right; *top:* 388, 386, 166; *bottom:* 266, 347, 185. Scale bars are 0.5 nA and 25 ms. The graphs show the voltage dependence of the population average intramembrane charge fitted to a Boltzmann equation. Parameters of each fit are from left to right; *top:* (Q_{max} in fC/pF, $V_{1/2}$ in mV, k in mV): 6.6, 12.1, 22; 5.9, 18, 23.2; 5.4, 21.8, 25.1; *bottom:* 5.5, 13. 3:17.8; 4.9, 20.1, 23.3; 5.9, 13.6, 18. Parameters of the fit of non-transfected cells (*squares*) are: 0.8, 11.2, 10.5. The experimental charge (mean ± SEM) at V_{test} = +100 mV was (in fC/pF) 6.4 ± 0.6 for WT; 5.5 ± 0.6 for Δ671–690; 5.2 ± 0.8 for Δ720–765; 5.5 ± 0.6 for Δ724–743; 4.8 ± 0.6 for Δ671–690/Δ720–765; and 6.1 ± 1.1 for Δ671–690/Δ724–743.

response to a 50-ms depolarization to +90 mV from a holding potential of −40 mV is shown in each panel. A second line-scan in some panels shows a Ca^{2+} transient activated by 10 mM caffeine in a myotube expressing the same construct. All line-scan images have a duration (x axis) of 2.05 s and a variable cell dimension (y axis) indicated in the figure legend. Line-scans were integrated across the y axis to obtain the time course of the average fluorescence change. The highest fluorescence intensity during 1.9 s following the depolarization, the peak fluorescence, is shown in each panel as a function of voltage. For WT, Δ671–690, and Δ671–690/Δ720–765, the mean peak fluorescence was fit to a Boltzmann equation indicated by the sigmoidal line. As shown by the top left and center panels of Fig. 3, Δ671–690 expressed a Ca^{2+} transient versus voltage relationship strikingly similar to that expressed by the control construct. Hence, the 671–690 region could not possibly have an essential role in the activation of Ca^{2+} transients in this expression system. This conclusion was further supported by a cell-by-cell analysis of the Boltzmann parameters (Table 1) compared to control (t-test significance p = 0.68, 0.98, 0.17 for $\Delta F/F_{max}$, $V_{1/2}$, and k, respectively). In contrast, Δ720–765 failed to evoke Ca^{2+} transients entirely (Fig. 3, *top right*). Consequently, the latter region of the II-III loop and not the 671–690 region was critical for triggering Ca^{2+} transients. The limit of fluorescence detection, based on microscope settings and the average resting fluo-4 fluorescence, was ~0.1 $\Delta F/F$ units; that is, we could detect an ~10% change above the cell resting fluorescence. Using a pseudo-ratiometric equation for estimating the cytosolic free Ca^{2+} and assuming a resting free Ca^{2+} of 100 nM (Conklin et al., 1999), the nominal limit of resolution of free Ca^{2+} change was ~200 nM; thus changes in free Ca^{2+} concentration under this limit could have taken place and would have escaped detection. Because Δ720–765 removes more than twice as many residues as Δ671–690, we tested the narrower α_{1S} 724–743 region, which also confers skeletal EC function to a cardiac α_{1C} subunit (Nakai et al., 1998). We found that Δ724–743, like the longer deletion of the same region,

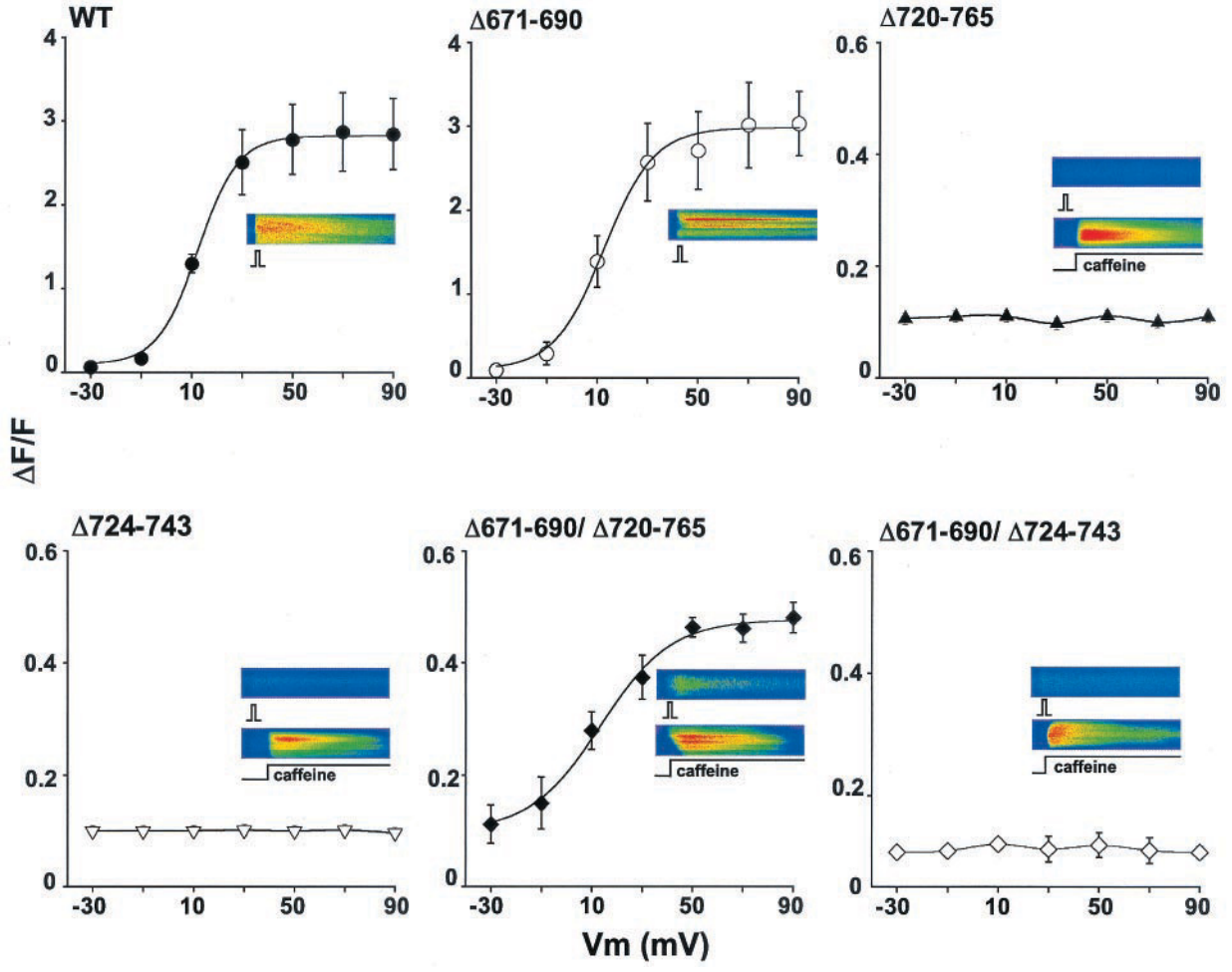

FIGURE 3 Ca^{2+} transients expressed by II-III loop deletions. The insets show confocal line-scan images of fluo-4 fluorescence in response to a 50-ms depolarization to +90 mV from a holding potential of −40 mV. Pseudo-colors cover four ΔF/units (blue < 0.2 to red > 4). The line-scan duration (x axis) was 2.05 s and the cell dimension (y axis) was (in μm) from left to right; *top:* 16.7, 48.8, 20.2; *bottom:* 25.7, 29.9, 86.9. In some panels a second line-scan shows a Ca^{2+} transient after perfusion with external solution containing 10 mM caffeine. The graphs show the population average voltage dependence of the Ca^{2+} transient measured in resting fluorescence units fitted to a Boltzmann equation. Parameters of each fit are from left to right; *top:* ($\Delta F/F_{max}$, $V_{1/2}$ in mV, k in mV): 2.7, 12.4, 7.9; 2.8, 12.2, 9.5; none; *bottom:* none; 0.38, 13.4, 14; none.

abolished Ca^{2+} transients entirely (Fig. 3, *bottom left*). Loss of Ca^{2+} transients could be due to a loss of Ca^{2+} storage capacity of the transfected cell, so to rule out this possibility cells expressing Δ720–765 or Δ724–743 were perfused with external solution supplemented with 10 mM caffeine. The insets in Fig. 3 show that caffeine evoked robust Ca^{2+} transients and thus the Ca^{2+} storage capacity of transfected cells was not adversely modified. The absence of Ca^{2+} transients in the presence of normal charge movements suggested that Δ724–743 and Δ720–765 expressed a DHPR in which the voltage sensor was truly uncoupled from SR Ca^{2+} release.

Residues 671–690 and 720–765 are the only two regions of the II-III loop that have been reported to screen positively for EC coupling-related functions, albeit by different techniques. We thus investigated whether voltage-evoked Ca^{2+} transients were expressed when both regions were removed from the II-III loop. Surprisingly, the bottom center panel of Fig. 3 shows that Δ671–690/Δ720–765 expressed Ca^{2+} transients that increased with depolarization and saturated at a maximum amplitude ($\Delta F/F_{max}$) ~20% of control. This result was highly consistent and was observed in 13 of 13 myotubes from three batches of cultured cells. Analysis of the voltage-dependence of the Ca^{2+} transient showed that neither the midpoint potential nor the steepness of the fluorescence versus voltage relationship was affected by this double deletion (Table 1). These results provide a clear indication that the skeletal DHPR has a latent EC coupling activity that is unmasked by simultaneous removal of residues 671–690 and 720–765. In molecular terms, the 720–765 region could be a conformation-sensitive region of the II-III loop stabilized by strong residue-residue interactions with other regions of the II-III loop. Thus, the loss of EC coupling produced by removal of residues 720–765 could

be the result of a conformation change that is partially reverted by a second conformational change in the II-III loop produced by removal of residues 671–690. To further test whether the latent EC coupling activity could have originated from additional regions of the II-III loop, we deleted all the sequence between the two deletions, namely, residues 671–765. Unfortunately, Δ671–765 failed to express charge movements, hence these data were not included in the present analysis. We also tested EC coupling recovery by Δ671–690/Δ724–743 (Fig. 3, *bottom right*). The results with the latter construct were far less consistent, and small Ca^{2+} transients ($\Delta F/F_{max}$~0.2) were only observed in 2 of 11 cells from three batches of cultured cells. The reasons for this inconsistency are not clear, especially since this double deletion removes fewer residues from the II-III loop than Δ671–690/Δ720–765.

We further investigated whether the Ca^{2+} current expressed by Δ671–690/Δ720–765 contributed to the triggering of the Ca^{2+} transient. Ca^{2+}-entry dependent EC coupling is normally not present in skeletal myotubes, but can be induced by expression of α_{1C} in dysgenic myotubes or modified DHPR β subunits in β null myotubes (Garcia et al., 1994; Sheridan et al., 2001). In the present case, such a mechanism could have been induced by an aberrant conformation of the α_{1S} protein carrying the two internal deletions. A straightforward pharmacological intervention consists of comparing Ca^{2+} transients in the presence and absence of inorganic Ca^{2+} channel blockers. However, these compounds are known to partially, yet significantly, depress voltage-evoked Ca^{2+} transients in skeletal myotubes (see Fig. 3A of Wilkens et al., 2000). To avoid this complication, we blocked the Ca^{2+} current by replacing a conserved pore glutamate by lysine at position 1014 in repeat III of α_{1S}. The E1014K substitution in a full-length α_{1S} was previously shown to abolish the inward Ca^{2+} current entirely, yet the magnitudes of the expressed Ca^{2+} transients were unaltered (Dirksen and Beam, 1999). In Fig. 4 *A* we compared whole-cell currents expressed by Δ671–690/Δ720–765 and Δ671–690/Δ720–765/E1014K in standard external solution containing 10 mM Ca^{2+} at the indicated potentials from a holding potential of −40 mV. In agreement with the previous results (Dirksen and Beam, 1999) inward currents during the pulse were entirely abolished by the E1014K substitution. To determine whether inward tail currents were present, the residual cell capacitance was subtracted with a −P/4 protocol. Selected voltage steps that activated large currents during the pulse, namely +30 mV for the Ca^{2+}-conducting construct and +70 for the pore mutant, were preceded by −P/4 pulses of the same duration and delivered from the same holding potential. Fig. 4 *B* shows difference currents after −P/4 subtraction at the two potentials indicated above and at −30 mV that did not activate ionic currents. The results indicated that inward tail currents were not present in the Δ671–690/Δ720–765/E1014K construct. The voltage dependence of the pulse current is shown in Fig. 4 *C*. Starting at +20 mV, the E1014K substitution unmasked a large outwardly rectifying current which in native Ca^{2+} channels is observed at much higher potentials (Hess et al., 1986). More importantly, inward current was not present in the E1014K construct over the entire range of voltages used to activate the Ca^{2+} transient. In Fig. 5 *A* we compare Ca^{2+} transients and whole-cell currents expressed in the same cell by Δ671–690/Δ720–765 and Δ671–690/Δ720–765/E1014K. The time course and amplitude of the Ca^{2+} transients were remarkably similar despite the presence of a measurable Ca^{2+} current in the Ca^{2+}-conducting construct and the absence of inward currents in the E1014K construct at all potentials. Furthermore, the voltage-dependence of the Ca^{2+} transient collected in several cells (Fig. 5 *B*) were indistinguishable (*t*-test significance $p = 0.13, 0.9, 0.38$ for $\Delta F/F_{max}$, $V_{1/2}$, and k, respectively). Thus, the EC coupling recovered by Δ671–690/Δ720–765 was strictly a Ca^{2+}-entry independent skeletal-type EC coupling.

The kinetics of SR Ca^{2+} release can be inferred from the time course of the Ca^{2+} transient measured in the presence of a Ca^{2+} buffer that eliminates fluorescence due to Ca^{2+} accumulation in the cytosol. In a Ca^{2+}-buffered internal solution, the rate of change of cytosolic Ca^{2+} approximates the net difference between the rate of SR Ca^{2+} release and the rate of cytosolic Ca^{2+} removal (Melzer et al., 1984). Furthermore, because the SR Ca^{2+} release rate is much faster than the Ca^{2+} removal rate, $d(\Delta F/F)dt$ immediately after the depolarization is dominated by the SR Ca^{2+} release rate (Melzer et al., 1984). Fig. 6 *A* shows Ca^{2+} transients obtained by integration of confocal line-scans in myotubes internally dialyzed with internal solution supplemented with 5 mM EGTA and 1 mM fluo-4 free acid present in the patch pipette. Due to the sharp diminution in the amplitude of the fluorescence signal produced by EGTA, we could only perform these experiments in cells transfected with the control construct and Δ671–690, which expressed comparatively large Ca^{2+} transients. In response to a 50-ms depolarization there was a rapid increase in cytosolic Ca^{2+} followed by an equally fast decay upon termination of the depolarization. The fast decay was followed by a much slower component that was completed in the time scale of seconds. The time course of the fast component is consistent with the rate of termination of SR Ca^{2+} release, which for short depolarizations has a time constant of tens of milliseconds in adult frog fibers (Simon et al., 1989). The slow component is consistent with Ca^{2+} removal stimulated by the Ca^{2+} pump, although this has not been determined. The rate of change of fluorescence during the depolarization, $d(\Delta F/F)/dt$, is shown in Fig. 6 *B* for a pulse to +90 mV. For both constructs there was a sharp increase in the rate of change of fluorescence followed by an equally fast decline while the pulse was at +90 mV. This result is entirely consistent with determinations in adult rat skeletal muscle and suggests the presence of fast rates of activation and

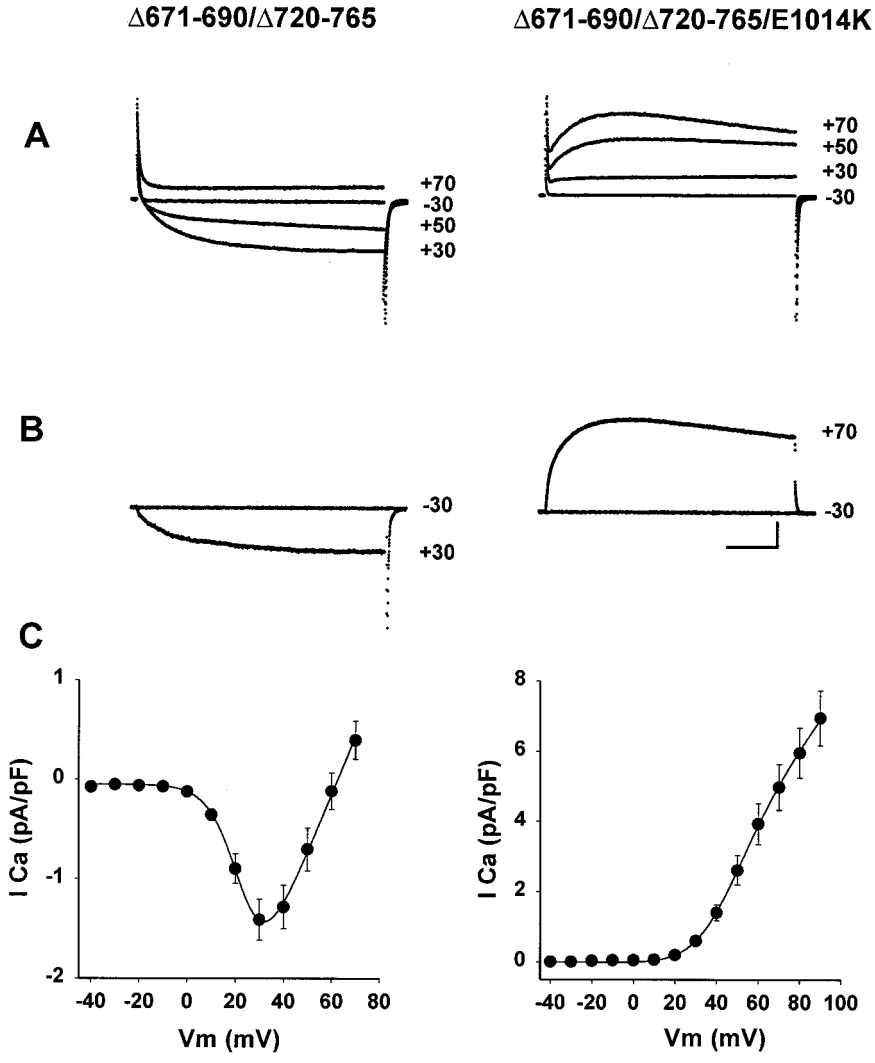

FIGURE 4 Current-voltage relationships expressed by Δ671–690/Δ720–765 with an additional E1014K pore mutation. (*A*) Whole-cell currents in standard Ca^{2+}-recording external solution are shown for a dysgenic myotube expressing Δ671–690/Δ720–765 (C = 347 pF) and a myotube expressing Δ671–690/Δ720–765/E1014K (C = 324 pF). Voltage steps were for 500 ms from a holding potential of −40 mV. Calibration bars are 500 pA and 100 ms. (*B*) The indicated voltage steps were preceded by 4 -P/4 pulses of the same duration from −40 mV. The P/4 subtracted traces are shown. (*C*) Population average current vs. voltage curves for five cells expressing each construct.

inactivation of SR Ca^{2+} release (Shirokova et al., 1996; Szentesi et al., 1997). Fig. 6 *C* shows the peak rate of fluorescence change during the upstroke of the depolarization for the control construct and Δ671–690 at two potentials. In both cases the rate of cytosolic Ca^{2+} increase was comparatively faster for Δ671–690 ($p < 0.05$). However, since the rate of fluorescence change and the confocal scan rate (2.05 ms per scan) were of the same magnitude, the results must be interpreted with caution. At the very least, these results indicate that the Ca^{2+} release rate expressed by Δ671–690 is not kinetically impaired. A submillisecond-scanning confocal microscope would be required to fully resolve the Ca^{2+} release rate expressed by this construct.

The voltage dependence of the Ca^{2+} conductance expressed by the II-III loop deletion constructs is shown in Fig. 7. In each panel the sigmoidal line shows a Boltzmann fit of the mean conductance and the inset shows whole-cell Ca^{2+} current in response to a voltage step to +30 mV from a holding potential of −40 mV. The endogenous dysgenic Ca^{2+} current (not shown) was detected in only 2 of 47 nontransfected myotubes analyzed at a resolution of ~20 pA/cell. This is a Ca^{2+} current of low-density and fast activation kinetics previously described in dysgenic myotubes (Adams and Beam, 1990) and, in our hands, is far more frequent in mice of a different genetic background (Strube et al., 1998). The maximum Ca^{2+} conductance, G_{max}, of the control construct was ~110 pS/pF with a half-activation potential of +25 mV (Fig. 7, *top left*). The mean G_{max} expressed by Δ671–690 (*top center*) was similar, although the half-activation potential was slightly more

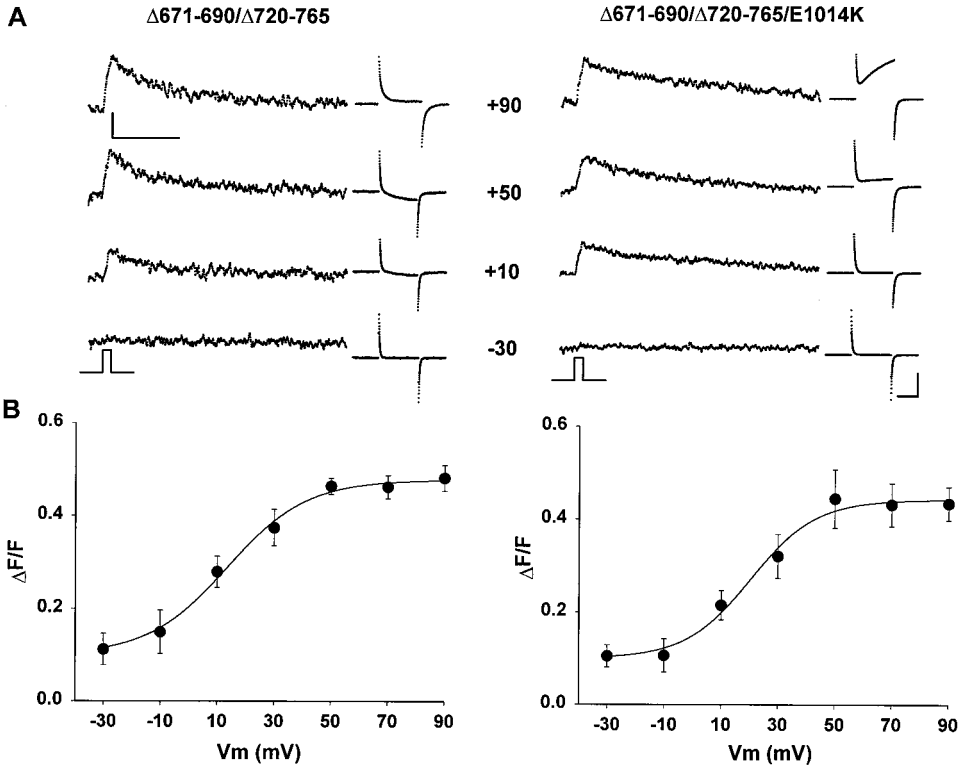

FIGURE 5 Skeletal-type EC coupling expressed by Δ671–690/Δ720–765/E1014K. (*A*) Confocal Ca^{2+} transients at the indicated potentials are shown for a dysgenic myotube expressing Δ671–690/Δ720–765 (C = 265 pF) and a myotube expressing Δ671–690/Δ720–765/E1014K (C = 284 pF). The time course of the transient was obtained by integration of line-scan images of fluo-4 fluorescence for 2.05 s. The 50-ms depolarization used to stimulate the Ca^{2+} transient is indicated by the square pulse and the whole-cell current during the depolarization is shown expanded next to the trace of florescence. Current calibration bars (25 ms, 1 nA) and fluorescence calibration bars (500 ms, 0.25 Δ*F*/*F*) are the same for both cells. (*B*) Population average Ca^{2+} transient versus voltage curves for five cells expressing each construct with Boltzmann parameters ($\Delta F/F_{max}$, $V_{1/2}$ in mV, *k* in mV) *left:* 0.38, 13.4, 14; *right:* 0.34, 20.3, 11.5.

positive. However, a cell-by-cell analysis (Table 1) did not reveal significant differences in any of the fitted Boltzmann parameters compared to control (*t*-test significance p = 0.72, 0.23, and 0.59 for G_{max}, $V_{1/2}$, and k, respectively). Ca^{2+} current was undetectable (<20 pA/cell) in the majority of myotubes expressing Δ720–765 or Δ724–743 (13 of 16 cells from six cultures and 8 of 11 cells from three cultures, respectively). However, in a few instances these two constructs expressed a measurable Ca^{2+} current of a magnitude ~4-fold lower than WT control (not shown). Because all cells analyzed expressed charge movements in a consistent manner (Table 1), the inability of these two constructs to express Ca^{2+} current was unrelated to the lack of targeting of DHPRs to the cell membrane. In contrast, the double deletion constructs expressed, in the majority of tested cells, a high-density Ca^{2+} current of approximately half the control density, ~60–70 pS/pF (Fig. 7, *bottom left* and *right*). Ca^{2+} current expression by Δ671–690/Δ720–765 and Δ671–690/Δ724–743 was observed in 5 of 7 cells from four cultures and 6 of 6 cells from three cultures, respectively. Two cells expressing the former construct failed to express Ca^{2+} current but expressed large charge movements, which are indicated in the figure legend. Ca^{2+} current expression by Δ671–690/Δ724–743 was observed consistently and this result was deemed highly significant since, at the same time, this construct consistently failed to trigger Ca^{2+} transients. Thus, there is a clear molecular distinction between the structural determinants of the Ca^{2+} current and those of EC coupling. In summary, the severe decrease in Ca^{2+} conductance produced by Δ724–743 and Δ720–765 agrees with previous observations showing that this region of the II-III loop controls expression of the L-type Ca^{2+} current and is critical for retrograde signaling from RyR1 to the DHPR (Grabner et al., 1999). However, the observation that the preponderance of cells transfected with Δ671–690/Δ720–765 and Δ671–690/Δ724–743 expressed a high-density Ca^{2+} current is difficult to explain within the boundaries of the present understanding of retrograde signaling (see Discussion).

A physical uncoupling of the DHPR and RyR1 occurs in RyR1 null myotubes, and this is manifested in the kinetics of activation of the L-type Ca^{2+} current, which is significantly faster in RyR1 null than in normal myotubes (Avila and Dirksen, 2000). Because Δ671–690/Δ724–743 was

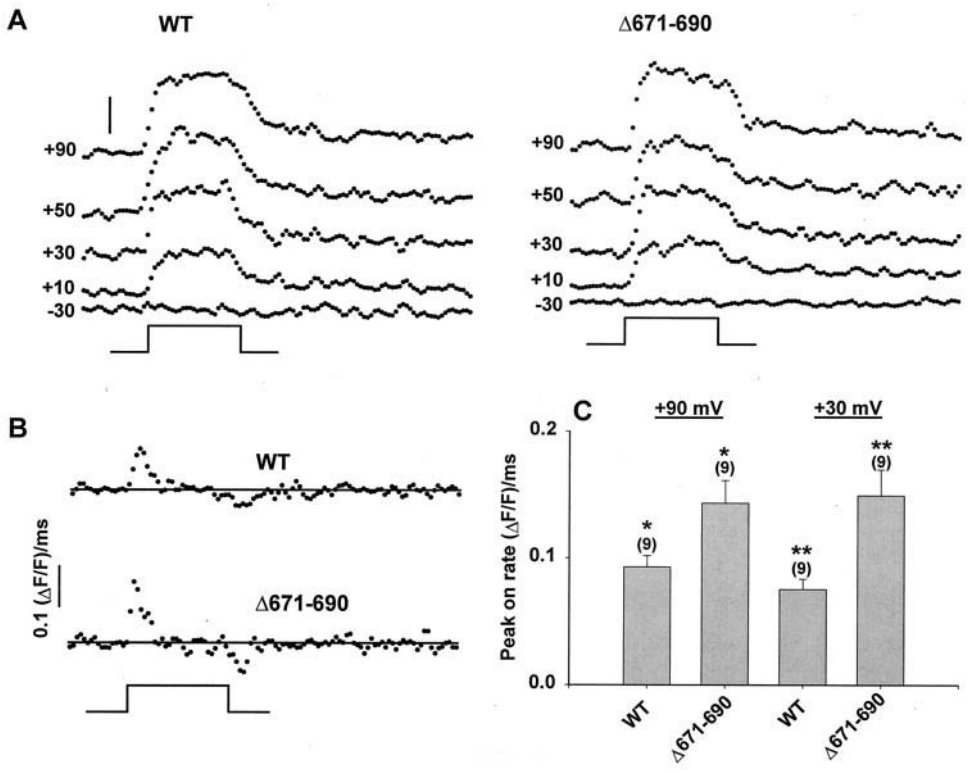

FIGURE 6 Rate of Ca^{2+} release expressed by Δ671–690. (*A*) Confocal Ca^{2+} transients at the indicated potentials are shown for a dysgenic myotube expressing full-length α_{1S} (C = 286 pF) and a myotube expressing Δ671–690 (C = 325 pF). The time course of the transient was obtained by integration of line-scan images of fluo-4 fluorescence. The 50-ms depolarization used to stimulate the Ca^{2+} transient is indicated by the square pulse. The internal (pipette) solution contained 5 mM EGTA and 1 mM fluo-4 free acid. Fluorescence calibration bar is 0.5 $\Delta F/F$. (*B*) Representative time derivatives of confocal Ca^{2+} fluorescence, in $\Delta F/F$ units, for a depolarization to +90 mV. (*C*) The peak rate of fluorescence change at the onset of the depolarization is shown at two potentials for the indicated number of cells. Data sets with *t*-test statistical significance $p < 0.05$ are shown by asterisks.

unable to couple voltage-sensing to SR Ca^{2+} release but Δ671–690/Δ720–765 produced a consistent EC coupling, we compared the kinetics of activation of the Ca^{2+} currents expressed by both constructs. Such an analysis could provide an indication of whether Δ671–690/Δ724–743 induces a physical separation of the DHPR and RyR1. Fig. 8 *A* shows scaled Ca^{2+} currents in response to a depolarization to +40 mV from a holding potential of −40 mV. In agreement with the previous study (Avila and Dirksen, 2000), we found that Ca^{2+} current activation was composed of a fast component followed by a much slower component during prolonged depolarization. In the current records (*gray traces*), the slow component is noticeable at times longer than 50 ms. The visual impression was confirmed by chi-square tests performed on monoexponential (χ^2 = 84 and 3.8 for RyR1 null and control, respectively) and biexponential (χ^2 = 0.21 and 1.88, respectively) fits and the latter are shown in Fig. 8 *A* by the dark lines. As shown by the histograms in Fig. 8 *B*, the fast and slow components of activation were comparatively faster in RyR1 null than in control myotubes, which is also in agreement with the previous study. The kinetics of activation of the Ca^{2+} current expressed by Δ671–690/Δ720–765, Δ671–690/Δ724–743, and Δ671–690 were not significantly different from control but significantly slower than the Ca^{2+} current of RyR1 null myotubes. Several statistical analyses of these data and the relative amplitude of the two components of the exponential fits are indicated in the figure legend. The kinetics of activation of the L-type Ca^{2+} current was previously suggested to vary with the level of expression of α_{1S} in myotubes (Adams et al., 1996). In Fig. 8, *C* and *D*, we plotted the fitted activation time constant as a function of the Ca^{2+} current density for each cell. These data show that within the range of Ca^{2+} current density achieved in the present study, namely 1–5 pA/pF, we did not find such a correlation for any of the constructs, either separately or pooled (R^2 = 0.21 and 0.18 for plots in Fig. 8, *C* and *D*, respectively). Hence, the similar activation kinetics of Δ671–690/Δ720–765, Δ671–690/Δ724–743, Δ671–690, and WT observed here are more likely to reflect inherent properties of the DHPR-RyR1 interaction rather than the level of maturity of the myotube. In summary, the kinetics of activation of the expressed L-type Ca^{2+} current strongly supports the view that the EC uncoupled phenotype of Δ671–690/Δ724–743 or the partially coupled phenotype of Δ671–690/Δ720–765 may not involve a physical separation of the DHPR and RyR1.

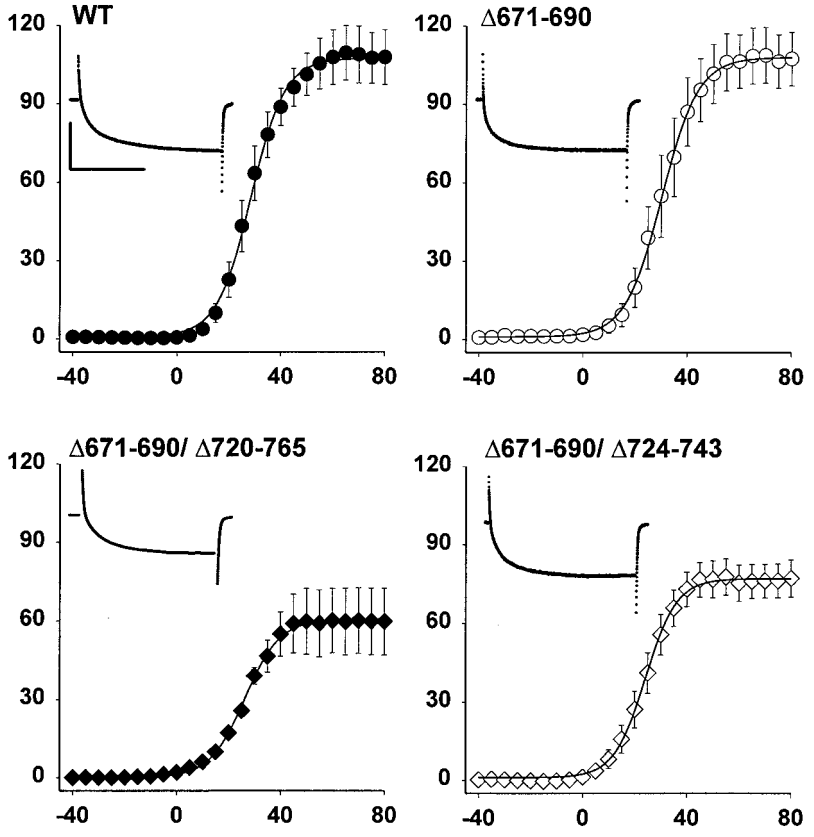

FIGURE 7 Ca^{2+} conductance expressed by II-III loop deletions. The insets shows whole-cell Ca^{2+} currents in dysgenic myotubes expressing the indicated construct. Δ720–765 and Δ724–743 did not express Ca^{2+} currents consistently and are not shown. The depolarizing potential was +30 mV for 500 ms from a holding potential of −40 mV. The capacitance of each cell (in pF) is from left to right; *top:* 247, 258; *bottom:* 314, 255. Scale bars are 1 nA and 250 ms. The graphs show the voltage dependence of the population average Ca^{2+} conductance fitted to a Boltzmann equation. Parameters of the fit (G_{max} in pS/pF, $V_{1/2}$ in mV, k in mV) are from left to right; *top:* 107.4, 28.4, 6.6; 108.1, 32.9, 7.1; *bottom:* 60.7, 31.3, 6.7; 77.1, 23.8, 6.2.

DISCUSSION

The main observations of the present work are as follows: 1) removal of α_{1S} II-III loop residues 671–690 does not eliminate the EC coupling and Ca^{2+} channel functions of the DHPR; 2) removal of α_{1S} residues 720–765 or residues 724–743 eliminates EC coupling entirely and most of the Ca^{2+} current; 3) removal of α_{1S} residues 720–765 and residues 671–690 partially but not entirely eliminates skeletal-type EC coupling and Ca^{2+} current; and 4) removal of α_{1S} residues 724–743 and residues 671–690 eliminates EC coupling entirely, but Ca^{2+} current only partially. Observations (1) and (2) allow us to conclude unambiguously that α_{1S} 720–765 is an EC coupling-sensitive region of the II-III loop, whereas α_{1S} 671–690 is dispensable. Also, (3) suggests that regions other than α_{1S} 671–690 and α_{1S} 720–765 are directly engaged in voltage-dependent activation of RyR1. Finally, (4) demonstrates that the Ca^{2+} channel and EC coupling functions of the DHPR have different molecular underpinnings.

Previously, functional expression studies in dysgenic cells were unable to demonstrate an influence of α_{1S} 671–790 in the EC coupling characteristics of myotubes when this region of α_{1S} was replaced by the homologous region of mammalian cardiac α_{1C} (Nakai et al., 1998) or replaced by a nonhomologous II-III loop of invertebrate origin (Wilkens et al., 2001). Furthermore, scrambling of the RKRRK binding motif of α_{1S} 671–790 (Proenza et al., 2000a) or complete deletion of the region (Ahern et al., 2001b) failed to significantly alter the skeletal EC coupling phenotype. However, in the present work, the removal of α_{1S} 671–790 was not entirely without consequence. Deletion of this region had an unforeseen positive effect of the kinetics of SR Ca^{2+} release and was critical for unmasking the new component of EC coupling observed in the absence of α_{1S} 720–765; hence α_{1S} 671–790 is neither functionally or structurally inert. The two experimental observations mentioned above are consistent with the view that the 671–790 region participates in negative control either slowing the rate of SR Ca^{2+} release or altogether blocking SR Ca^{2+} release initiated by signals elsewhere in the DHPR. We realize, however, that a proposed inhibitory function of the 671–690 region is in sharp contrast with the stimulatory effect of the 671–690 peptide on RyR1 channels reported in several studies

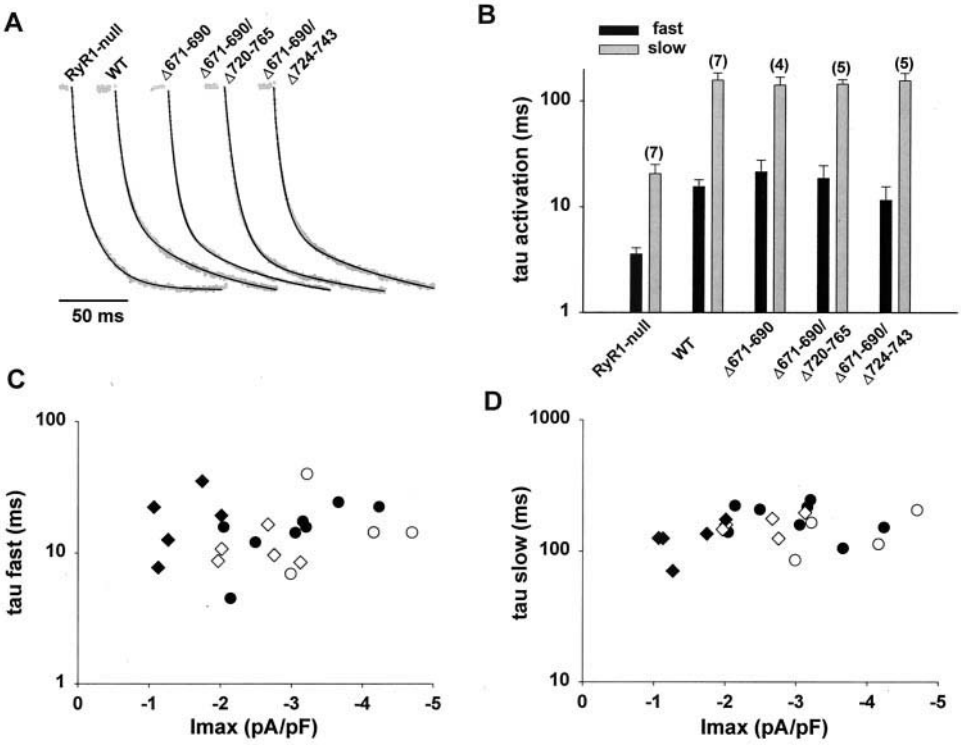

FIGURE 8 Kinetics of activation of the Ca^{2+} current expressed by II-III loop deletions. (*A*) Normalized whole-cell Ca^{2+} current (*gray traces*) during a depolarization to +40 mV from a holding potential of −40 mV. The pulse duration was 500 ms and only the initial 120 ms are shown. The first 16 ms of the trace were omitted. The line is a biexponential fit of the pulse current 16 ms after the onset of the pulse with fast and slow time constants, in ms, from left to right: 2.7, 16.1; 15.7, 165; 31.9, 165; 13.9, 135; 8.7, 159. The pre-exponential factors of the fast and slow components were, respectively, from *left* to *right:* 0.26, 0.74; 0.62, 0.38; 0.51, 0.49; 0.46, 0.54; 0.5, 0.5. (*B*) Averages of the fitted fast and slow activation time constants (mean ± SE) for the indicated number of cells. All data (fast versus slow time constants) had *t*-test significance $p < 0.05$. Activation time constants of RyR1 null and WT (fast versus fast and slow versus slow time constants) were significantly different (*t*-test significance $p < 0.05$). Activation time constants of WT control and II-III loop deletion constructs (fast versus fast and slow versus slow) were not significantly different (ANOVA significance $p > 0.23$). The average (mean ± SE) pre-exponential factors of the fitted fast and slow components for the same cells were 0.29 ± 0.06 and 0.71 ± 0.14 for RyR1 null; 0.34 ± 0.08 and 0.66 ± 0.16 for WT; 0.35 ± 0.1 and 0.65 ± 0.18 for Δ671–690; 0.46 ± 0.12 and 0.54 ± 0.14 for Δ671–690/Δ720–765; 0.45 ± 0.13 and 0.55 ± 0.16 for Δ671–690/Δ724–743. (*C*, *D*) Time constants of activation are plotted as a function of the maximum Ca^{2+} current density of each cell. Black circles (WT), open circles (Δ671–690), black diamonds (Δ671–690/Δ720–765), open diamonds (Δ671–690/Δ724–743).

(cited in the Introduction). It is important to keep in mind that RyR1 channels respond to many different kinds of ligands (see Table 2 of Coronado et al., 1994), including charged ligands such as polylysine (El-Hayek and Ikemoto, 1998). We would thus speculate that the lysine/arginine RKRRK motif of the 671–690 peptide might have contributed to overrepresent the stimulatory activity of the α_{1S} 671–690 peptide over and above that of other II-III loop peptides tested (Saiki et al., 1999; Stange et al., 2001).

The critical participation of α_{1S} 720–765 in EC coupling, the region previously identified by functional screening of α_{1C}/α_{1S} chimeras, was reaffirmed by the present results. However, the data also showed that a signal capable of triggering skeletal-type EC coupling was generated elsewhere when α_{1S} 720–765 and α_{1S} 671–690 were absent. It could be argued that the double α_{1S} 671–690/720–765 deletion produced artifactual interactions with RyR1 and that these interactions, normally not present between α_{1S} and RyR1, would be responsible for the recovered EC coupling. This possibility is considered highly unlikely due to three fundamental reasons. First, the Boltzmann parameters of charge movement expressed by the double deletion construct and those expressed by the control construct are statistically undistinguishable (*t*-test significance $p > 0.12$). Hence the trigger signal itself was not altered. Second, except for the maximum amplitude of the Ca^{2+} transient, the midpoint potential and the steepness factor k of the Ca^{2+} transient versus voltage curve were identical to controls. Therefore, the characteristics of the outgoing signal that activates the Ca^{2+} transient were only partially modified. Finally, the kinetics of the expressed Ca^{2+} current was identical to that expressed by the control construct. Consequently, retrograde signaling from the RyR1 to the DHPR was not modified. None of these results is consistent with the presence of artifactual interactions. Of these results, the slow biphasic Ca^{2+} current recovered by Δ671–690/720–765, with a kinetics of activation similar to the control Ca^{2+} current (Fig. 8), was deemed especially significant. It has

been argued that α_{1S} 720–765 modulates expression of the Ca^{2+} current by retrograde signaling from the RyR1 to the DHPR. The recovery of more than half of the control Ca^{2+} conductance by Δ671–690/720–765 and by Δ671–690/724–743 demonstrates that this region of the II-II loop is unlikely to harbor a unique signal controlling Ca^{2+} current expression. Instead of a signaling domain, the 720–765 region could be a conformation-sensitive "permissive" region controlling protein folding. Disruption of proper protein folding by deletion of residues in this region could impair EC coupling signals generated elsewhere in the DHPR. Alternatively, α_{1S} 720–765 may be one of several regions involved in bidirectional signaling between the DHPR and RyR1. The latter explanation is highly attractive because it also implies that different DHPR-RyR1 coupling domains could trigger SR Ca^{2+} release perhaps independently of each other. Such a model could provide a basis for understanding the phenotype of the Δ671–690/Δ724–743 construct and the fact that the 720–765 region is functionally unique.

The mechanism by which EC coupling is eliminated by removal of α_{1S} 720–765 and recovered by removal of α_{1S} 720–765 and α_{1S} 671–690 is reminiscent of the electrostatic interactions that hold the voltage sensor of the *Shaker* K^+ channel in a functional state (Papazian et al., 1995). This study showed that some charge neutralization mutations in the S4 transmembrane segment block protein folding. In these cases, channel function can be rescued by a second charge neutralization in S2 or S3. The functional rescue by double mutations suggested that S4 forms a strong network of local electrostatic charges with other transmembrane domains. The observation in the *Shaker* K^+ channel is directly applicable to the II-III loop, which contains several loci of electrostatic charge within α_{1S} 671–690 and α_{1S} 720–765 and also outside these two regions. For example, D^{744}DEEDE^{749} could form a lattice of negative electrostatic charges stabilized by a lattice of positive charges provided by R^{681}KRRK^{685} (see Fig. 1 *A*). Removal of α_{1S} 720–765 would thus require removal of α_{1S} 671–690 for maintenance of II-III loop stability. The same example would explain why the EC coupling loss produced by Δ724–743, which does not remove D^{744}DEEDE^{748}, cannot be rescued by further deletion of α_{1S} 671–690. However, this model would not explain why Δ671–690 alone does not disrupt EC coupling. It could be that D^{744}DEEDE^{749} or other charged residues in the 720–765 region can be equally well-stabilized by charges inside and outside the 671–690 region. A study of charge-charge interactions in the II-III loop by mutagenesis and functional expression is clearly required to provide an explanation consistent with all results.

Potential EC coupling domains outside the II-III loop have been identified in the carboxyl terminus of α_{1S} and the carboxyl terminus of the β1a subunit of the DHPR. The carboxyl terminus of α_{1S} binds to RyR1, inhibits RyR1 channels incorporated in planar bilayers, and participates in targeting the DHPR to junctions containing RyR1 (Slavik et al., 1997; Proenza et al., 2000b; Flucher et al., 2000; Morales et al., 2001). DHPR β1 is critical for expression of Ca^{2+} current, charge movements, Ca^{2+} transients, and Ca^{2+} sparks of correct morphology (Beurg et al., 1999a, b; Conklin et al., 1999). Additional observations identified the participation of the C-termini of β1a in EC coupling under conditions in which the density of DHPR voltage sensors expressed in the plasma membrane was not a limiting factor (Beurg et al., 1999b; Sheridan et al., 2001). Whether these regions contribute to EC coupling in the absence of the α_{1S} 720–765 region of the II-III loop remains an attractive possibility. Finally, it is important to point out that although the fluorescence signal generated by Δ671–690/Δ720–765 is small, this result cannot be taken as an argument favoring the notion that the bulk of the EC coupling is initiated by the II-III loop and that a minor component is initiated outside of the II-III loop. A previous report indicates that ~80% of the EC coupling fluorescence signal can also be eliminated, under conditions of normal charge movement, by deletions within the DHPR β_{1a} subunit in the context of an otherwise wild-type DHPR (Beurg et al., 1999b; Sheridan et al., 2001). Hence, the output signal leaving the DHPR receives contributions from more than one subunit and, by nature, is nonadditive. The relative contribution to EC coupling of different domains within the DHPR is a challenging issue that needs to be addressed in the future.

This work was supported by National Institutes of Health Grants AR46448 and HL47053, and by predoctoral fellowships from American Heart Association to C.A.A.

REFERENCES

Adams, B. A., and K. G. Beam. 1990. A novel calcium current in dysgenic skeletal muscle. *J. Gen. Physiol.* 94:429–444.

Adams, B. A., T. Tanabe, and K. G. Beam. 1996. Ca^{2+} current activation rate correlates with alpha 1 subunit density. *Biophys. J.* 71:156–162.

Ahern, C. A., J. Arikkath, P. Vallejo, C. A. Gurnett, P. A. Powers, K. P. Campbell, and R. Coronado. 2001b. Intramembrane charge movements and excitation-contraction coupling expressed by two-domain fragments of the Ca^{2+} channel. *Proc. Natl. Acad. Sci. U.S.A.* 98:6935–6940.

Ahern, C. A., D. Bhattacharya, L. Mortenson, and R. Coronado. 2001a. Deletion analysis of two domains of the dihydropyridine receptor II-III loop involved in excitation-contraction coupling. *Biophys. J.* 80:377*a*. (Abstr.).

Avila, G., and R. T. Dirksen. 2000. Functional impact of the ryanodine receptor on the skeletal muscle L-type Ca^{2+} channel. *J. Gen. Physiol.* 115:467–480.

Beurg, M., C. A. Ahern, P. Vallejo. P. A. Powers, R. G. Gregg, and R. Coronado. 1999b. Involvement of the carboxy-terminus region of the dihydropyridine receptor β1a subunit in excitation-contraction coupling of skeletal muscle. *Biophys. J.* 77:2953–2967.

Beurg, M., C. Sukhareva, M. W. Ahern, J. A. Conklin, C. Powell, P. A. Powers, R. G. Gregg, and R. Coronado. 1999a. Differential control of skeletal muscle Ca^{2+} current and excitation-contraction coupling by the dihydropyridine receptor β subunit. *Biophys. J.* 76:1744–1756.

Beurg, M., M. Sukhareva, C. Strube, P. A. Powers, R. G. Gregg, and R. Coronado. 1997. Recovery of Ca^{2+} current, charge movements, and Ca^{2+} transients in myotubes deficient in dihydropyridine receptor β_1 subunit transfected with β_1 cDNA. *Biophys. J.* 73:807–818.

Block, B. A., T. Imagawa, K. P. Campbell, and C. A. Franzini-Armstrong. 1988. Structural evidence for direct interaction between the molecular

components of the transverse tubule/sarcoplasmic reticulum junction in skeletal muscle. *J. Cell Biol.* 107:2587–2600.

Casarotto, M. G., F. Gibson, S. M. Pace, S. M. Curtis, M. Mulcair, and A. F. Dulhunty. 2000. A structural requirement for activation of skeletal ryanodine receptors by peptides of the dihydropyridine receptor II-III loop. *J. Biol. Chem.* 275:11631–11637.

Chandler, W. K., R. F. Rakowski, and M. F. Schneider. 1976. Effects of glycerol treatment and maintained depolarization on charge movement in skeletal muscle. *J. Physiol.* 254:285–316.

Conklin, M., P. Powers, R. G. Gregg, and R. Coronado. 1999. Ca^{2+} sparks in embryonic mouse skeletal muscle selectively deficient in dihydropyridine receptor α_{1S} or $\beta 1$ subunits. *Biophys. J.* 76:657–669.

Coronado, R., J. Morrissette, M. Sukhareva, and D. M. Vaughan. 1994. Invited review: structure and function of ryanodine receptors. *Am. J. Physiol. Cell Physiol.* 266:C1485–C1504.

Dirksen, R. T., and K. G. Beam. 1999. Role of calcium permeation in dihydropyridine receptor function. Insights into channel gating and excitation-contraction coupling. *J. Gen. Physiol.* 114:393–403.

Dulhunty, A. F., D. R. Laver, E. M. Gallant, M. G. Casarotto, S. M. Pace, and S. Curtis. 1999. Activation and inhibition of skeletal RyR channels by a part of the skeletal DHPR II-III loop: effects of DHPR Ser-687 and FKBP12. *Biophys. J.* 77:189–203.

El-Kayek, R., B. Antoniu, J. P. Wang, S. L. Hamilton, and N. Ikemoto. 1995. Identification of calcium release-triggering and blocking regions of the II-III loop of the skeletal muscle dihydropyridine receptor. *J. Biol. Chem.* 270: 22116–22118.

El-Kayek, R., and N. Ikemoto. 1998. Identification of the minimum essential region in the II-III loop of the dihydropyridine receptor $\alpha 1$ subunit required for activation of skeletal muscle-type excitation-contraction coupling. *Biochemistry.* 37:7015–7021.

Flucher, B. E., N. Kasielke, and M. Grabner. 2000. The triad targeting signal of the skeletal muscle calcium channel is located in the COOH terminus of the α_{1S} subunit. *J. Cell Biol.* 151:467–477.

Franzini-Armstrong, C., and F. Protasi. 1997. Ryanodine receptors of striated muscles: a complex channel capable of multiple interactions. *Physiol. Rev.* 77:699–729.

Garcia, J., T. Tanabe, and K. G. Beam. 1994. Relationship of calcium transients to calcium currents and charge movements in myotubes expressing skeletal and cardiac dihydropyridine receptors. *J. Gen. Physiol.* 103: 125–147.

Grabner, M., R. T. Dirksen, and K. G. Beam. 1999. The II-III loop of the skeletal muscle dihydropyridine receptor is responsible for the bi-directional coupling with the ryanodine receptor. *J. Biol. Chem.* 274:21913–21919.

Gurrola, G. B., C. Arevalo, R. Sreekumar, A. J. Lokuta, J. W. Walker, and H. H. Valdivia. 1999. Activation of ryanodine receptors by imperatoxin and a peptide segment of the II-III loop of the dihydropyridine receptor. *J. Biol. Chem.* 274:7879–7886.

Hess, P., J. B. Lansman, and R. W. Tsien. 1986. Calcium channel selectivity for divalent and monovalent cations. Voltage and concentration dependence of single channel current in ventricular heart cells. *J. Gen. Physiol.* 88: 293–319.

Kim, A. M., and J. L. Vergara. 1998. Fast gating of Ca^{2+} release in frog skeletal muscle revealed by supercharging pulses. *J. Physiol.* 511.2: 509–518.

Leong, P., and D. H. MacLennan. 1998. The cytoplasmic loops between domains II and III and domains III and IV in the skeletal muscle dihydropyridine receptor bind to a contiguous site in the skeletal muscle ryanodine receptors. *J. Biol. Chem.* 273:29958–29964.

Lu, X., L. Xu, and G. Meissner. 1994. Activation of the skeletal muscle calcium release channel by a cytoplasmic loop of the dihydropyridine receptor. *J. Biol. Chem.* 269:6511–6516.

McPherson, P. S., and K. P. Campbell. 1993. The ryanodine receptor/Ca^{2+} release channel. *J. Biol. Chem.* 268:13765–13768.

Meissner, G. 1994. Ryanodine receptor/Ca^{2+} release channels and their regulation by endogenous effectors. *Annu. Rev. Physiol.* 56:485–508.

Melzer, W., E. Rios, and M. F. Schneider. 1984. The time course of calcium release and removal in skeletal muscle fibers. *Biophys. J.* 45:637–641.

Morales, J., P. Pate, J.-Z. Zhang, and S. L. Hamilton. 2001. Interaction of the carboxyl-terminal of the alpha 1 subunit of the skeletal muscle DHPR with the calmodulin binding site on RyR1. *Biophys. J.* 80:379*a*. (Abstr.).

Nakai, J., T. Tanabe, T. Konno, B. Adams, and K. G. Beam. 1998. Localization in the II-III loop of the dihydropyridine receptor of a sequence critical for excitation-contraction coupling. *J. Biol. Chem.* 273:24983–24986.

O'Reilly, F. M., and M. Ronjat. 1999. Direct interaction of the skeletal dihydropyridine receptor $\alpha 1$ subunit with skeletal and cardiac ryanodine receptors. *Biophys. J.* 76:466*a*. (Abstr.).

Papazian, D. M., X. M. Shao, S.-A. Seoh, A. F. Mock, Y. Hiang, and D. H. Wainstock. 1995. Electrostatic interactions of S4 voltage sensor in Shaker K^+ channels. *Neuron.* 14:1293–1301.

Perez-Reyez, E., and T. Schneider. 1994. Calcium channels: structure, function, and classification. *Drug Dev. Res.* 33:295–418.

Proenza, C., C. M. Wilkens, and K. G. Beam. 2000a. Excitation-contraction coupling is not affected by scrambled sequence in residues 681–690 of the dihydropyridine receptor II-III loop. *J. Biol. Chem.* 275:29935–29937.

Proenza, C., C. Wilkens, N. M. Lorenzon, and K. G. Beam. 2000b. A carboxyl-terminal region important for the expression and targeting of the skeletal muscle dihydropyridine receptor. *J. Biol. Chem.* 257:23169–23174.

Rios, E., and G. Pizarro. 1991. Voltage sensor of excitation-contraction coupling in skeletal muscle. *Physiol. Rev.* 71:849–908.

Saiki, Y., R. El-Hayek, and N. Ikemoto. 1999. Involvement of the Glu724-Pro760 region of the dihydropyridine receptor II-III loop in skeletal muscle excitation-contraction coupling. *J. Biol. Chem.* 274:7825–7832.

Sheridan, D., W. Cheng, C. A. Ahern, P. Vallejo, P. A. Powers, and R. Coronado. 2001. Truncation of skeletal DHPR $\beta 1a$ subunit results in mixed voltage and Ca^{2+} dependent excitation-contraction coupling. *Biophys. J.* 80:376*a*. (Abstr.).

Shirokova, N., J. Garcia, G. Pizarro, and E. Rios. 1996. Ca^{2+} release from sarcoplasmic reticulum compared in amphibian and mammalian skeletal muscle. 107:1–18.

Simon, B. J., M. G. Klein, and M. F. Schneider. 1989. Caffeine slows turn-off of calcium release in voltage clamped skeletal muscle fibers. *Biophys. J.* 55:793–797.

Slavik, K. J., J.-P. Wang, B. Aghdasi, J.-Z. Zhang, F. Mandel, N. Malouf, and S. L. Hamilton. 1997. A carboxy-terminal peptide of the $\alpha 1$-subunit of the dihydropyridine receptor inhibits Ca^{2+} release channels. *Am. J. Physiol. Cell Physiol.* 272:C1475–C1481.

Stange, M., A. Tripathy, and G. Meissner. 2001. Two domains in the dihydropyridine receptor activate the skeletal muscle Ca^{2+} release channel. *Biophys. J.* 81:1419–1429.

Strube, C., M. Beurg, P. A. Powers, R. G. Gregg, and R. Coronado. 1996. Reduced Ca^{2+} current, charge movement and absence of Ca^{2+} transients in skeletal muscle deficient in dihydropyridine receptor $\beta 1$ subunit. *Biophys. J.* 71:2531–2543.

Strube, C., M. Beurg, C. Sukhareva, J. A. Ahern, C. Powell, P. A. Powers, R. G. Gregg, and R. Coronado. 1998. Molecular origin of the Ca^{2+} current of skeletal muscle myotubes selectively deficient in dihydropyridine receptor β_1 subunit. *Biophys. J.* 75:207–217.

Sutko, J. J., and J. A. Airey. 1996. Ryanodine receptor Ca^{2+} release channels: does diversity in form equal diversity in function? *Physiol. Rev.* 76: 1027–1071.

Szentesi, P., V. Jacquemond, L. Kovacs, and L. Csernoch. 1997. Intramembrane charge movement and sarcoplasmic reticulum calcium release in enzymatically isolated mammalian skeletal muscle fibers. *J. Physiol.* 505.2: 371–384.

Takekura, H., L. Bennett, T. Tanabe, K. G. Beam, and C. Franzini-Armstrong. 1994. Restoration of junctional tetrads in dysgenic myotubes by dihydropyridine receptor cDNA. *Biophys. J.* 67:793–803.

Tanabe, T., K. G. Beam, B. A. Adams, T. Niidome, and S. Numa. 1990. Regions of the skeletal muscle dihydropyridine receptor critical for excitation-contraction coupling. *Nature.* 346:567–572.

Wilkens, C. M., N. Kasielke, B. E. Flucher, K. G. Beam, and M. Grabner. 2001. Excitation-contraction coupling is unaffected by drastic alteration of the sequence surrounding residues L-720-L764 of the α_{1S} II-III loop. *Proc. Natl. Acad. Sci. U.S.A.* 98:5892–5897.